Journal Pre-proof

Coupling metabolomics analysis and DOE optimization strategy towards enhanced IBDV production by chicken embryo fibroblast DF-1 cells

Jia Lin, Xiaoping Yi, Yingping Zhuang

PII: S0168-1656(19)30906-X

DOI: https://doi.org/10.1016/j.jbiotec.2019.10.018

Reference: BIOTEC 8535

To appear in: *Journal of Biotechnology*

Received Date: 18 July 2019

Revised Date: 17 October 2019

Accepted Date: 27 October 2019

Please cite this article as: Lin J, Yi X, Zhuang Y, Coupling metabolomics analysis and DOE optimization strategy towards enhanced IBDV production by chicken embryo fibroblast DF-1 cells, *Journal of Biotechnology* (2019), doi: https://doi.org/10.1016/j.jbiotec.2019.10.018

Coupling metabolomics analysis and DOE optimization strategy towards enhanced IBDV production by chicken embryo fibroblast DF-1 cells

Jia Lin[1], Xiaoping Yi[1*], Yingping Zhuang[1]

Affiliations:

1. State Key Laboratory of Bioreactor Engineering, East China University of Science and Technology (ECUST), Shanghai, People's Republic of China.

*Corresponding author. E-mail: xpyi@ecust.edu.cn

Highlights

This study describes in detail the metabolic effects of IBDV on DF-1 cells.
A method is proposed to verify metabolite analysis using statistical strategies.
An optimized medium is proposed to produce IBDV vaccines based on DF-1 cells.

Abstract: Infectious bursal disease (IBD) caused by IBD virus (IBDV) is highly contagious viral and vaccination in chicken embryo has been an effective mean to prevent acute infection. However, the current production of IBDV vaccine faces serious batch instability and external contamination. The chicken embryonic fibroblast cell line DF-1 is widely used for the proliferation of avian viruses and vaccine production. Thus, optimizing the production of IBDV by DF-1 cells has an important application value. Combining metabolomics analysis and a Design of Experiments (DOE) statistical strategy, this study successfully optimized the process of IBDV production by DF-1 cells. Differential analysis and time series analysis of metabolite data in both IBDV-infected and uninfected DF-1 cells were performed by multivariate statistical analysis. The results showed that the intracellular metabolite intensities of glycolysis, the pentose phosphate pathway, the nucleoside synthesis pathway, lipid metabolism, and glutathione metabolism were upregulated, and the TCA cycle underwent a slight downregulation after IBDV infection of DF-1 cells. Based on the metabolome results and DOE statistical optimization method, the additive components suitable for IBDV proliferation were determined. The IBDV titer increased by 20.7 times upon exogenous addition of cysteine, methionine, lysine and nucleosides in the control medium, which is consistent with the predicted result (20.0 times) by a multivariate quadratic equation. This study provides a strategy for the efficient production of IBDV vaccines and could potentially be utilized to improve the production of other viral vaccines and biologics.

Key words: DF-1; IBDV; metabolome; DOE methodology

1 Introduction

Infectious bursal disease (IBD), caused by infectious bursal disease virus (IBDV), is a highly contagious viral and acute infection with tropism for lymphoid tissue that has been striking chicken flocks for more than fifty years and exerting a considerable economic impact on the global poultry industry (Muller et al., 2003). IBDV, a small molecule and non-enveloped virus, belongs to the genus *Avibirnavirus* of the *Birnaviridase* family with a nonenveloped icosahedral capsid (55-60 nm in diameter) containing a double-stranded RNA genome consisting of two segments (A and B) (Ingrao et al., 2013). Vaccination is the main approach to prevent and treat IBDV. Although various vaccine forms, such as subunit vaccine (Liu et al., 2005), DNA vaccine (Hulse and Romero, 2004), and genetically engineered live IBDV vaccines (Noor, 2009), have been developed due to technological innovation, conventional live and inactivated IBDV vaccines are still widely used (Muller et al., 2012). However, the virus propagation is performed in chicken embryos with the risk of batch instability and external pollution, and the embryo lethal dose50 (ELD50) of the obtained IBDV ranged from $10^{-4.50}$/0.4 ml to $10^{-7.40}$/0.4 ml (Li et al., 2015). Chicken embryo fibroblasts (CEF) cells are used for IBDV reproduction, but they have a finite *in vitro* life span and the preparation of the cells is high cost, and tedious, laborious. The obtained IBDV titer from CEF cells is approximately 6.3 TCID50/0.1 ml, while it was approximately 7.3 TCID50/0.1 ml from DF-1 cells (Rekha et al., 2014). Therefore, DF-1 cells become a prospective cell line of avian origin to replace CEF for continuous demands.

The chicken embryonic fibroblast cell line DF-1 has been widely applied in the production of several avian virus vaccines due to the lack of endogenous fragments associated with avian leukosis virus and sarcoma virus (Schaefer-Klein et al., 1998), such as Marek's disease virus (Levy et al., 2005) and avian influenza virus (Lee et al., 2008; Moresco et al., 2010). Increasing attention has been paid on the interactions between avian viruses and their host cells. Niu *et al.* and Luo *et al.* studied the transcriptomic changes of DF-1 cells inoculated with avian reovirus (Niu et al., 2017) or avian influenza virus (Luo et al., 2018) to further understand the antiviral response and phenotypes of histopathological changes of DF-1 cells after viral infection. Chen *et al.* performed small RNA deep sequencing in Newcastle disease virus-infected DF-1 cell to reveal that cellular miRNAs affect virus replication by controlling host-virus interaction (Chen et al., 2019). Those studies investigate the interaction between the virus and host DF-1 cells on the molecular level, while this study will further understand the actual behavior of virus-controlled DF-1 cell from the perspective of metabolic regulation.

Metabolome has been widely used in the field of industrial biotechnology in recent years (Dietmair et al., 2012a; Guan et al., 2014; Wang et al., 2015). Metabolites can indicate the phenotypes of the actual process, which means small changes in gene expression or protein activity often induce a larger change in metabolites, and then the metabolites changes are responsible for cell or tissue behavior directly whilst also influencing proteome and transcriptome (Dietmair et al., 2012b; Klein and Heinzle, 2012). Therefore,

metabolome can provide a large amount of information about the definitions of biological process phenotypes and biosystems. In recent years, the application of metabolite analysis methods to study the effects of viral infection on cell metabolism has become more widespread. Munger *et al.* have used LC-MS analysis to study changes in the cellular metabolite levels after human cytomegalovirus (HCMV) infection of human fibroblasts, demonstrating that HCMV significantly disrupts cellular metabolic homeostasis and institutes its own specific metabolic program (Munger et al., 2006). Since then, increasingly more studies have shown that viral infections activate many cellular metabolic processes (Hollenbaugh et al., 2011; Vastag et al., 2011). With the continuous innovation of detection technology, the metabolome is increasingly more widely used in virus-induced disease research—for example, to identify therapeutic targets for viral-induced diseases (Delgado et al., 2012), establish appropriate cell disease research models (Cui et al., 2017), and investigate the effects of drugs on viral-induced diseases (Beale et al., 2019). However, application of the metabolome in viral vaccine production has rarely been reported (Silva et al., 2016). Combing the analysis results of the metabolome with the design of experiments (DOE) methodology which has been verified before (Lin et al., 2019), we have already obtained an optimized medium suitable for virus propagation, which provides a potential strategy for the optimization of the production of the virus vaccine.

In this study, we investigated the changes in the intracellular metabolites between DF-1 cells infected by IBDV and the control cells as well as the time series analysis of DF-1 intracellular metabolites after IBDV infection to understand the metabolic changes of DF-1 cells after IBDV infection. On one hand, the metabolomics research will provide informative insights into the prevention and treatment of IBDV. On the other hand, in our previous study, we observed that amino acid metabolism and lipid metabolism exerted important effects on the growth of DF-1 cells based on the intracellular metabolome of DF-1 cells in different media (Lin et al., 2019), so we investigated metabolite changes in DF-1 cells infected by IBDV to further understand the relationship between virus and host DF-1 cells on the metabolic level in this study. The statistical analysis of the metabolite results would reveal the key components affecting the reproduction of IBDV in DF-1 cells, which provides clues for the optimization of the virus production medium and thereby efficient production of the IBDV vaccine.

2 Materials and methods

2.1 DF-1 and IBDV culture

Routine cell culture of adherent DF-1 cells was performed in Nunc EasYFlask 25-cm^2 flasks (Thermo Scientific, USA) with 5 mL of DMEM/F12 (1:1) (Gibco, USA) with 5% fetal bovine serum (Biological Industries, USA) in a humidified incubator at 37 ℃ with 5% CO_2. The cell number and viability were determined using Countstar (ALIT Life Science, CN), an automated Trypan blue cell counter. DF-1 cells were infected with IBDV in flasks when the cells reached a confluence of 90%, and the cells were harvested when 80% of the cells showed lesions, followed by determination of the virulence using

$TCID_{50}$.

$TCID_{50}$ assay was performed as previously described (Chen et al., 2018; He et al., 2016). Monolayers of DF-1 cells in 96-well plates was infected with 0.1ml of 10-fold serial dilutions (10^{-1}-10^{-10}) of viral samples. Six replicate wells of a 96-well cell culture plate were used for each dilution. The cytopathic effect (CPE) characterized by cytoplasmic, cell rounding, detachment and lysis was observed under a microscopy and the titrations were calculated as a 50% tissue culture infective dose ($TCID_{50}$) using the Reed-Muench method (Reed and Muench, 1938). The relative titer was calculated as the following equation:

$$\text{Relative Titer}=10^{[\log_{10}(TCID_{50,sample})-\log_{10}(TCID_{50,control})]}$$

where $TCID_{50,\ control}$ is the average virus titer at 36 hpi in control media, and $TCID_{50,\ sample}$ is the sample virus titer.

2.2 Metabolite sample acquisition, detection and analysis

For metabolome analysis of global biochemical profiles, the cells were cultivated in Nunc EasYFlask 75 cm^2 with 15 mL of medium and were infected by IBDV when the cells reached a confluence of 90%. A total of 10^7 cells was harvested and stored at -80℃ immediately after washing in ice-cold phosphate-buffered saline, and three of these samples were used to determine the intracellular metabolites at each time point (t=6, 12, 18, and 36 hours post infection, hpi). Additionally, metabolite determination was performed by Metabolon, Inc. (Durham, NC) using standard protocols. Metabolon developed a platform that integrates chemical analysis, metabolite identification and relative quantification, data reduction, and quality assurance components of the process. Individual cell samples (n=3 per group) were extracted and split into equal parts for analysis by GC/MS and UPLC-MS/MS. The methodology is detailed elsewhere (Lawton et al., 2008). Prior to statistical analysis, the data obtained were normalized to the protein concentration by Bradford analysis. All identified metabolite relative abundance matrices were uploaded on MetaboAnalysis (http://www.metaboanalyst.ca) for multivariate data statistics and Pathway Analysis (Chong et al., 2018; Xia and Wishart, 2016).

2.3 DOE methodology

In this study, the experimental design was used to optimize the virus production medium based on the metabolome. First, the Plackett-Burman design (PBD) was used to screen the components that significantly influenced the target (IBDV titer). Second, the path of the steepest ascent design was used to determine the component concentration ranges. Third, the Box-Behnken Design (BBD) was used to determine the final concentration in the optimal media. Finally, the effectiveness of the optimized medium was determined in a verification experiment. The experimental method design matrix, including PBD and BBD, and the significance analysis of the restrictive analysis of the experimental data, were performed by Design Expert 10.0.6.

2.3.1 Plackett-Burman design

In this study, PBD was used to screen the factors that significantly affected cell growth from nineteen metabolites to harvest the maximum IBDV titer and was classified into 8 categories, as listed in Table 3 according to possible pathways. Each variable was tested at two levels—high (+1) and low (-1)—which were initially experimentally estimated in DMEM/F12 (1:1). In summary, eleven independent variables (eight of the abovementioned variables and three dummy variable) were screened by twelve trial runs according to PBD with N=11. Further details regarding the PBD matrix are listed in Table 4.

2.3.2 Path of the steepest ascent design

The path of the steepest ascent design was designed to identify the optimal range of values. The three most significant factors were obtained from the PBD experiment and their center points were determined by the path of the steepest ascent design for response surface analysis. More details are listed in Table 5.

2.3.3 Box-Behnken design

Response surface analysis applied BBD to evaluate the effects of three independent variables on cell growth to achieve an increased maximum IBDV titer. Using the other factors maintained in DMEM/F12 (1:1), we studied the three significant variables at the three coded levels: high (+1), intermediate (0) and low levels (-1). To determine the optimum values for the three selected variables, 15 trial runs were designed by BBD and included 3 replicates. The experimental matrix, including the experimental and predicted results, is provided in Table 6.

The following second-order polynomial model fits the relationship between the response and test variable. The equation obtained using statistical methods is as follows:

$$Y=\beta_0+\sum_{i=1}^{3}\beta_i X_i+\sum_{i=1}^{3}\beta_{ii} X_i^2+\sum_{i=1}^{2}\sum_{j=i+1}^{3}\beta_{ij} X_i X_j$$

where Y is the predicted response, and β_0, β_i, β_{ii}, and β_{ij} are the constant, linear coefficient, quadratic coefficient and interaction coefficient, respectively. X_i and X_j are the independent variables.

2.3.4 Validation of the fitting model

The second-order polynomial described above was used to direct the experiment to validate the fitted model. IBDV was cultured in optimized medium to validate the optimization results using the statistical strategy for the maximum IBDV titer as the targets compared with cells cultured in DMEM/F12 (1:1) medium as the control.

2.4 Method matrix and ANOVA

The experimental method matrix was designed throughout the process, including by PBD and BBD, and restricted analysis of all the experimental data was performed using Design Expert 10.0.4 (Stat-Ease Inc., Minneapolis, USA). The statistical significance of the variables was evaluated by applying analysis of variance (ANOVA) using Student's t-test. The adequacy of the model was verified using Fisher's F-test.

3 Results and discussion

3.1 Metabolome differential and time series analysis based on multivariate statistical analysis

When DF-1 cells were cultured to a confluency of approximately 80%, spent medium was replaced by fresh DMEM/F12(1:1) medium containing 1% fetal calf serum and IBDV was inoculated. The control group was treated with an equivalent of phosphate buffer solution instead of IBDV. Cell counting was performed every 6 hours. DF-1 cell growth was significantly changed after inoculation with IBDV (Fig. 1A). In the control group without IBDV, the cells still grew normally. In the experimental group inoculated with IBDV, after a short-term increase of 6 hours, the cells began to show a significant downward trend, and the growth difference between the experimental and control groups became increasingly larger. According to the principle of "no obvious difference", "beginning difference", "differential difference beginning to be obvious" and "maximum difference", and the time node of IBDV infection and replication process reported in the reference (Hui and Leung, 2015), the four time points of 6 hpi, 12 hpi, 18 hpi and 36 hpi were selected to investigate the effect of IBDV infection on the intracellular metabolites of DF-1 cells.

3.1.1 Multivariate statistical analysis of intracellular metabolites in DF-1 cells inoculated with IBDV and the control group

According to the cell growth changes after IBDV infection and time of virus infection and replication, ten million cells were collected at 6 hpi, 12 hpi, 18 hpi and 36 hpi. Metabolite group detection was performed using three parallel groups at each time point. The experimental process covered IBDV infection, replication, assembly and secretion. In total, 193 intracellular metabolites were determined and included amino acids, peptides, carbohydrates, lipids, nucleotides, coenzymes and vitamins. LC/MS and GC/MS were used for analysis to ensure the accuracy of the results. The principal component analysis (PCA) results (Fig. 1B) showed that the structure and quality of the data represented the close relationship among the biological repeated groups. The samples were distinguished between the experimental and control groups along the sampling times, indicating that the metabolite group could monitor the culture process of virus-infected cells. According to the principle of "no significant difference at 6 hpi, difference occurred at 12 hpi, 18 hpi, and significant difference at 36 hpi", statistical analysis was performed on the experimental and control groups at each time point. We used fold change values (FC, no IBDV/IBDV) and p values to evaluate each metabolite. When the fold change value range was less than 0.5 or greater than 2, and the p value was less than 0.1, 14 different metabolites were obtained (Table 1). The metabolic pathways in which these 14 metabolites were mainly involved include the carbohydrate, lipid, amino acid, vitamin and cofactor relative pathways. When the FC value was lower than 0.5, the intracellular metabolite levels of glycerol 3-phosphate, GPC, citrulline, fructose, and glucose were significantly higher in DF-1 cells inoculated with IBDV than in DF-1 cells without IBDV. These metabolites were mainly involved in lipid metabolism, arginine, proline metabolism, and carbohydrate metabolism in DF-

1 cells. Other metabolites were significantly downregulated in DF-1 cells infected with IBDV and were involved in the glycine, serine, and threonine metabolic pathways, pantothenic acid and CoA metabolic pathways, lysine metabolic pathways, pentose metabolic pathways, and some carbohydrate-related pathways. To determine the important roles of arginine, proline, glycine, serine, threonine and lysine in the propagation of IBDV, further analysis would be carried out by DOE methodology.

3.1.2 Time series analysis of intracellular metabolites of DF-1 cells infected by IBDV

The time-series intracellular metabolites of DF-1 cells infected with IBDV were analyzed to investigate the metabolites or metabolic pathways in DF-1 cells after IBDV infection. Using the metabolites of DF-1 cells infected with IBDV at 0 hpi, the metabolite samples of 5 time points was used to investigate changes in the intracellular metabolites before and after IBDV infection. We used hierarchical cluster analysis in 5 sample groups (Fig. 1C). The result between the 0 hpi and 6 hpi samples was not significantly different because IBDV had just started to infect DF-1 cells. Partial Least Square analysis (Fig. 1D) identified 15 metabolites with the highest-ranking calculated VIP. The intracellular intensity of xylitol, inosine, malate, gluconate, erythronate, proline, hypoxanthine, glucuronate, N-carbamoyl-aspartate, fumarate, and N-acetylserine gradually decreased with virus propagation, while the intracellular intensity of cysteine, glycerol 3-phosphate, and glycerophosphorylcholine GPC gradually increased. The gradually decreasing metabolites were mostly involved in glycogen synthesis, the pentose pathway and nucleoside metabolism. The intracellular intensity of glucose gradually increased with time, indicating that the glucose utilization pathway changed. Additionally, the increase in the intensity of metabolites associated with lipid metabolism pathways emphasized the important roles of lipid metabolism in the process of virus reproduction.

With further analysis of the metabolic pathways of intracellular metabolites in DF-1 cells infected with DF-1 cells over time, the significant metabolites were integrated into the KEGG pathway database, and the resulting "metabolome view" showed all the significant pathway by pathway abundance analysis based on p-value (Table 2). Through the pathway analysis of pathways, the metabolic pathways with significant differences according to the time ($p<0.01$) and impact over 0.18 were selected. The results showed that the importance of amino acid metabolism, especially that of arginine, proline, cysteine, methionine, alanine, aspartic acid, glutamine, glycine, serine, threonine, histidine and lysine. Additionally, carbohydrate-related metabolism, lipid metabolism, and nucleoside metabolism changed significantly, which was consistent with the differential analysis and time series analysis of metabolites above mentioned.

3.2 Effect of IBDV infection on the metabolic pathway of DF-1 cells

Multivariate statistical analysis of the intracellular metabolites of DF-1 cells infected by IBDV showed that IBDV affected the metabolism of DF-1 cells via multiple metabolic pathways, including central carbon metabolism, nucleoside metabolism, lipid metabolism, glutathione metabolism, and

amino acid metabolism.

3.2.1 Central carbon metabolism

Differential analysis and time series analysis showed significant changes in carbohydrate metabolism. Many studies have reported that viruses alter the metabolic state of cells, including glycolysis and nucleotide biosynthetic pathways (Munger et al., 2006). In this study, intracellular glucose uptake was significantly increased after IBDV infection, and glycolysis-related metabolites increased at 12, 18, and 36 hpi (Fig. 2). Compared with no IBDV infection in DF-1 cells, the intracellular intensity of glucose, glucose-6-phosphate, fructose-1, 6-diphosphate (Isobar), DHAP, 3-phosphglycerate and lactate significantly increased after IBDV infection, and the difference reached a peak at 36 hpi.

Regarding the pentose phosphate pathway, the intracellular intensities of the pentose phosphate pathway intermediate metabolites ribose-5-phosphate, ribulose/xylulose-5-phosphate, and ribose in IBDV-infected DF-1 cells were significantly higher than those in control cells, indicating that the pentose phosphate pathway played an important role in the proliferation of IBDV in DF-1 cells (Fig. 2). The pentose phosphate pathway provides precursors for nucleotide synthesis, which may imply an important function of nucleotide metabolism in the reproduction of IBDV.

The TCA cycle is very important for the energy production of cells. However, the intermediate metabolite intensities of α-ketoglutarate, succinate, fumarate, and malate were decreased in IBDV-infected DF-1 cell compared with those in the control group, indicating that IBDV propagation in DF-1 cells was less dependent on the TCA cycle where the carbon flux of glucose was reduced but in other metabolic pathways was increased (Fig. 2). Considering the intracellular metabolite pools changes in the glycolysis and the TCA cycle, the energy metabolism of DF-1 cells was changed after IBDV infection.

In this study, we found that IBDV infection promoted glycolysis in DF-1 cells by metabolome analysis, while Quan *et al*. analyzed the transcriptome in vvIBDV infected with B. lymphoblastic DT40 cells to find that the MAPK p38 signaling pathway was significantly upregulated, inhibiting the PI3K/Akt/mTOR signaling pathway (Quan et al., 2017) and implying that Aktl1 inhibited glycolysis by inhibiting GLUT1 expression. This may be because DT40 cells, as lymphocytes, sustained long-term infection (Delgui et al., 2009), while IBDV infection in DF-1 cells was acute and intense. Thus, IBDV has different effects on glycolysis in different cells, which had a similar phenomenon of HIV-infection in CD4+ T cells and macrophages (Hollenbaugh et al., 2011).

3.2.2 Lipid metabolism

In differential and time series analyses, we found that most of the lipid metabolites were increased significantly with the proliferation of IBDV in DF-1 cells, particularly glycerophospholipid metabolism ($p=1.89\times10^{-9}$, impact = 0.24; Table 2) and sphingolipid metabolism ($p = 6.80 \times 10^{-7}$, impact = 0.30, Table 2). Compared with the corresponding metabolite levels in the control group, the levels of metabolites in DF-1 cells with IBDV infection increased significantly over time, especially at 36 hpi (Fig. 3).

Metabolome analysis showed that IBDV induced significant upregulation of most intracellular lipid-related metabolic pathways in DF-1 cells. IBDV is a non-enveloped RNA virus; however, lipid metabolism is still important for IBDV to multiply in DF-1 cells. It was reported that the metabolism of glycerophospholipids was related to the replication of viruses. The progeny reproduction of some viruses is formed between the endoplasmic reticulum and lipid droplets and requires the host to provide a large amount of triacylglycerol to form a lipid membrane, making a compartment for the replication and synthesis of viral RNA (Sanchez and Lagunoff, 2015; Schaefer and Chung, 2013). Additionally, the intracellular intensities of DHAP (Fig. 2) and glycerol 3-phosphate (Fig. 3) were upregulated in DF-1 cells infected by IBDV. The virus was reported to switch DHAP to G3P in a shuttle pathway catalyzed by glycerol-3-phosphate dehydrogenase (GPDH), which shifted the carbon metabolism to the synthesis of glycerophosphoric acid (Schoeman et al., 2016). The activity of sphingolipid metabolism further proved that sphingolipid metabolism was involved in the de novo synthesis of lipid rafts. Additionally, inhibition of sphingolipid metabolism led to inhibition of the replication of HCV in its interaction with infected cells (Hirata et al., 2012; Sakamoto et al., 2005). Hui *et al.* used RNA-Seq to detect transcriptome changes in caIBDV-infected DF-1 cells, and found that lipid membrane-associated regulatory factors LIPA and CH25H were overexpressed, while STARD4, LSS, and AACS were inhibited, altering the cell membrane fluidity and rearranging the lipid rafts of infected cells to ease the entry of IBDV into DF-1 cells (Hui and Leung, 2015) and facilitate the assembly and budding of viral particles (Yip et al., 2012). Therefore, changes in lipid metabolism not only facilitate the entry of IBDV into cells but also provide a suitable environment for the replication of IBDV.

3.2.3 Amino acid metabolism

Amino acids are highly abundant metabolites in cells and the main components of protein synthesis. We found that the intensities of many amino acids, including cysteine, lysine and methionine, involved in many metabolic pathways were changed in the metabolome (Fig. 4 A-C). For example, cysteine is involved in the synthesis of glutathione, and methionine involves in the formation of nucleosides (Avila et al., 2004; Conrad, 2014; ŽIvkov BaloŠ et al., 2019). The significant differences in the metabolic pathways of cystine and methionine indicate the important role of the relevant pathways. Additionally, glutamine, asparagine, alanine, serine, and threonine were reported to be beneficial for maintaining the genetic stability of the IBDV capsid protein VP2 in continuous passage in chicken embryo fibroblasts (CEFs) (Noor et al., 2014). In the above-mentioned time series analysis and differential analysis, the amino acid metabolism showed important roles.

Additionally, we found that glutathione-related metabolite pools gradually increased with the proliferation of IBDV in DF-1 cells ($p=4.9\times10^{-9}$; Impact=0.59; Table 2), and the increase in the cysteine pool induced by IBDV suggested the importance of glutathione metabolism. Fig. 4D shows that the intensity of most glutathione-related metabolites was significantly upregulated with IBDV proliferation

in DF-1 cells, and the difference between the experimental and control group reached a peak at 36 hpi. When we compared the intermediate metabolites of glutathione synthesis, cysteine-glutathione disulfide, cysteinylglycine, and 5-oxoproline in the experimental and control groups, the intensities of these metabolites increased after IBDV infection, indicating that IBDV stimulates the glutathione-related metabolic pathway related to oxidative stress when it was propagated in DF-1 cells and may play important roles in redox homeostasis, cell apoptosis (Li et al., 2019), and the phosphorylation state of various enzymes (Xiong et al., 2017) after IBDV infection in DF-1 cells.

3.2.4 Nucleoside metabolism

The metabolome analysis results showed that the numbers of intracellular DL-1 cells infected with IBDV, nucleosides and their synthetic precursors in the experimental group were generally higher than those in the control group (Fig. 5A), and a significant increase in intercellular pentose phosphate pathway metabolite pools was mentioned above, illustrating the important role of nucleoside synthesis for viral reproduction. IBDV induced a significant increase in the nucleoside synthesis metabolite pools in DF-1 cells, and the methionine pool increased to facilitate the methylation of nucleosides and mature nucleoside synthesis, as confirmed by the increased levels of intracellular methionine sulfoxide and S-adenosylmethionine (SAM) pools (Fig. 5 B-C). Lin *et al.* used microarray to detect the transcriptome of IBDV-infected chicken dendritic cells and found a large enrichment of RNA polymerase II(Lin et al., 2016), indicating an increase in intracellular RNA metabolite pools was necessary for IBDV proliferation.

3.3 Optimization of IBDV propagation medium based on metabolite analysis and the DOE method

Based on intracellular metabolite differential analysis and time series analysis of IBDV-infected DF-1 cell, amino acids, nucleosides, carbohydrate and lipid-related metabolic pathways were identified as the significant pathways in IBDV proliferation. However, since DF-1 cells have limitations in glucose uptake as the previous experimental results (data not shown), optimizing the concentration of glucose in the medium has no significant effect on IBDV propagation. In terms of lipid-related metabolic pathway, the mixture of lipids or triacylglycerol were considered as the exogenous lipid supplements, but those lipid components were dissolved in ethanol which has serious toxic effects on DF-1 cells. In the experimental medium, fetal bovine serum was the lipids provider and a small amount of serum were reported to be benefit to virus production (Liste-Calleja et al., 2014; Shen et al., 2012), and the current serum content was considered to satisfy the IBDV proliferation. Therefore, in our DOE experiments, amino acids and nucleosides-related components were optimized.

In the DOE experiments, components that might promote IBDV virus propagation in DF-1 cells were classified according to their constituent properties and pathways with similar function in the KEGG pathway database. Table 3 shows the optimized medium components (Table 3) and coding level for PBD. To obtain the maximum IBDV titer, PBD was performed on the eight components or groups obtained in the above analysis. The experimental design and results are shown in Table 4. The resulting restricted

model, with a P value of 0.0371 and an F value of 4.62, indicated that the model was of good predictive ability. The amino acid 6 (cysteine and methionine) group significantly affected the IBDV titer, and the amino acid 7 (lysine) and nucleoside groups also contributed significantly to the proliferation of IBDV in DF-1 cells (Table 3). Therefore, subsequent interactions among the three components or groups were further optimized to obtain an optimal medium that can promote IBDV production in DF-1 cells.

The path of steepest ascent design is an experimental design method that optimizes the appropriate concentration step size of the components. The three most important factors obtained from the PBD experimental results were further optimized along the path of the steepest ascent to determine their center point and then were used in the response surface analysis. Based on the results of the PBD experiment, the amino acid 6 group, the amino acid 7 group and the nucleoside group had positive effects on IBDV proliferation in DF-1 cells. Therefore, the concentrations of the three groups moved along the path of increasing concentration. In total, 5 gradient levels were set, while the concentrations of the other substances remained at the basal level. The experimental design and results are shown in Table 4. When the concentrations of amino acid group 6, amino acid group 7 and nucleosides reached 0.4 mM, 0.00225 mM and 1.25 mM, respectively, the harvested IBDV titers reached the highest level. Thus, these values were set as the central point of the subsequent BBD experiment.

Based on the path of the steepest ascent design results, BBD was performed to identify the interactions among significant factors and determine the optimal level of the three significant factors. The design process and results are shown in Table 6 and Figure 6. Variance analysis of the restriction model showed that the F value of the model was 6.29, and $p=0.028<0.05$, indicating that the results based on the quadratic equation model to obtain the maximum virus titer were significant; the analytical coefficient was $R^2=0.9188$, indicating the correlation between measured and predicted values was fitted well, and the Adj R2 results indicated that the model interpreted 77.27% of the variance. Although the individual effects of amino acid 6, amino acid 7 and nucleoside groups on the proliferation of IBDV in DF-1 cells were not all significant, the interaction effects and optimal levels of variables were determined by plotting the response surface curves. The interaction and optimization levels of the variables were determined according to the points of the response surface, and the correlation coefficient were obtained from the restriction analysis of the multivariate quadratic equation as follows:

Relative Titer=19.7025 + 0.487966 × A + 0.482753 × B + 2.03346 × C + 0.90351 × AB + 2.29574 × AC -0.434905 × BC -5.51458 × A^2 -6.6997 × B^2 -4.5946 × C^2

where A, B and C represent the coding levels of the amino acid 6 group, amino acid 7 group and nucleoside group, respectively.

The three-dimensional analysis of the response surface indicates that the model has a maximum unique solution, as shown in Figure 6(ABC). The predicted highest virus titer was increased by 20.0 times at amino acid 6=0.098, amino acid 7=0.034, nucleosides=0.245, and the corresponding component

concentrations were 0.410 mM, 0.002 mM and 1.311 mM, respectively. Compared with the control medium, the final IBDV titer increased by 20.7 times in the optimized medium (Fig. 6D, 36 hpi), consistent with the predicted result and indicating a significant improvement. The IBDV titer was 6.83 $TCID_{50}$/0.1 ml in control medium, and 8.14 $TCID_{50}$/0.1 ml in optimized medium (36 hpi). At the same time, comparing the growth of DF-1 cells in the control and optimized medium, the reduction of the viable cell density caused by IBDV-induced cell death was slowed down in the optimized medium, which provided a more durable environmental and a better material and energy preparation for the IBDV propagation. Therefore, IBDV reproduction was significantly improved in the optimized medium. This result confirmed again the important roles of cysteine, methionine, lysine and nucleosides in IBDV proliferation in DF-1 cells.

4 Conclusion

This study demonstrated the metabolic effects of IBDV on DF-1 cells based on a metabolomic analysis system and multivariate statistical analysis, indicating that IBDV infection enhanced the intracellular metabolite intensities of glycolysis, the pentose phosphate pathway, the nucleoside synthesis pathway, lipid metabolism, and glutathione metabolism while decreased the intracellular intensities of the TCA cycle metabolites in DF-1 cells. Based on the DOE statistical optimization method, the medium suitable for IBDV reproduction was established. Compared with the control medium, IBDV reproduction in optimized medium was significantly improved, and the titer was increased by 20.7 times, similar to the predicted result (20.0 times), which emphasized the importance of cysteine, methionine, lysine, and nucleosides. This study provides a streamlined strategy to optimize the viral propagation medium based on the metabolome to promote IBDV vaccine production and could potentially be utilized in the improvement of other viral vaccines and biologics production.

Declaration of interests

Jia Lin, Xiaoping Yi, and Yingping Zhuang declare that they have no known competing financial interests or personal relationships that could have appeared to influence the work reported in this paper.

Conflict of interest

No conflict of interest.

Acknowledgements

This study was funded by the Chinese National Programs for High Technology Research and Development (2015AA020801).

References

Avila, M.A., et al. 2004. Methylthioadenosine. *Int J Biochem Cell Biol*. 36,2125-2130.https://doi.org/10.1016/j.biocel.2003.11.016.

Beale, D.J., et al. 2019. Untargeted metabolomics analysis of the upper respiratory tract of ferrets following influenza A virus infection and oseltamivir treatment. *Metabolomics*. 15,33.https://doi.org/10.1007/s11306-019-1499-0.

Chen, G., et al. 2018. Antigenicity characterization of four representative natural reassortment IBDVs isolated from commercial three-yellow chickens from Southern China reveals different subtypes co-prevalent in the field. *Vet Microbiol*. 219,183-189.https://doi.org/10.1016/j.vetmic.2018.04.024.

Chen, Y., et al. 2019. MicroRNA Expression Profiling in Newcastle Disease Virus-Infected DF-1 Cells by Deep Sequencing. *Front Microbiol*. 10,1659.https://doi.org/10.3389/fmicb.2019.01659.

Chong, J., et al. 2018. MetaboAnalyst 4.0: towards more transparent and integrative metabolomics analysis. *Nucleic Acids Res*. 46,W486-W494.https://doi.org/10.1093/nar/gky310.

Conrad, N.K. 2014. The emerging role of triple helices in RNA biology. *Wiley Interdiscip Rev RNA*. 5,15-29.https://doi.org/10.1002/wrna.1194.

Cui, L., et al. 2017. Serum Metabolomics Investigation of Humanized Mouse Model of Dengue Virus Infection. *J Virol*. 91.https://doi.org/10.1128/JVI.00386-17.

Delgado, T., et al. 2012. Global metabolic profiling of infection by an oncogenic virus: KSHV induces and requires lipogenesis for survival of latent infection. *PLoS Pathog*. 8,e1002866.https://doi.org/10.1371/journal.ppat.1002866.

Delgui, L., et al. 2009. The capsid protein of infectious bursal disease virus contains a functional α4β1 integrin ligand motif. *Virology*. 386,360-372.https://doi.org/10.1016/j.virol.2008.12.036.

Dietmair, S., et al. 2012a. Metabolite profiling of CHO cells with different growth characteristics. *Biotechnol Bioeng*. 109,1404-1414.https://doi.org/10.1002/bit.24496.

Dietmair, S., et al. 2012b. A multi-omics analysis of recombinant protein production in Hek293 cells. *PLoS One*. 7,e43394.https://doi.org/10.1371/journal.pone.0043394.

Guan, N., et al. 2014. Comparative metabolomics analysis of the key metabolic nodes in propionic acid synthesis in Propionibacterium acidipropionici. *Metabolomics*. 11,1106-1116.https://doi.org/10.1007/s11306-014-0766-3.

He, X., et al. 2016. Role of naturally occurring genome segment reassortment in the pathogenicity of IBDV field isolates in Three-Yellow chickens. *Avian Pathol*. 45,178-186.https://doi.org/10.1080/03079457.2016.1139687.

Hirata, Y., et al. 2012. Self-enhancement of hepatitis C virus replication by promotion of specific sphingolipid biosynthesis. *PLoS Pathog*.

8,e1002860.https://doi.org/10.1371/journal.ppat.1002860.

Hollenbaugh, J.A., et al. 2011. Metabolite profiles of human immunodeficiency virus infected CD4+ T cells and macrophages using LC-MS/MS analysis. *Virology*. 415,153-159.https://doi.org/10.1016/j.virol.2011.04.007.

Hui, R.K., and F.C. Leung. 2015. Differential Expression Profile of Chicken Embryo Fibroblast DF-1 Cells Infected with Cell-Adapted Infectious Bursal Disease Virus. *PLoS One*. 10,e0111771.https://doi.org/10.1371/journal.pone.0111771.

Hulse, D.J., and C.H. Romero. 2004. Partial protection against infectious bursal disease virus through DNA-mediated vaccination with the VP2 capsid protein and chicken IL-2 genes. *Vaccine*. 22,1249-1259.https://doi.org/10.1016/j.vaccine.2003.09.021.

Ingrao, F., et al. 2013. Infectious Bursal Disease: a complex host-pathogen interaction. *Dev Comp Immunol*. 41,429-438.https://doi.org/10.1016/j.dci.2013.03.017.

Klein, S., and E. Heinzle. 2012. Isotope labeling experiments in metabolomics and fluxomics. *Wiley Interdiscip Rev Syst Biol Med*. 4,261-272.https://doi.org/10.1002/wsbm.1167.

Lawton, K.A., et al. 2008. Analysis of the adult human plasma metabolome. *Pharmacogenomics*. 9,383-397.https://doi.org/10.2217/14622416.9.4.383.

Lee, C.W., et al. 2008. Evaluation of chicken-origin (DF-1) and quail-origin (QT-6) fibroblast cell lines for replication of avian influenza viruses. *J Virol Methods*. 153,22-28.https://doi.org/10.1016/j.jviromet.2008.06.019.

Levy, A.M., et al. 2005. Marek's disease virus Meq transforms chicken cells via the v-Jun transcriptional cascade: A converging transforming pathway for avian oncoviruses. *Proceedings of the National Academy of Sciences of the United States of America*.

102,14831-14836.https://doi.org/10.1073/pnas.0506849102.

Li, C., et al. 2019. Glutamine starvation inhibits snakehead vesiculovirus replication via inducing autophagy associated with the disturbance of endogenous glutathione pool. *Fish Shellfish Immunol*. 86,1044-1052.https://doi.org/10.1016/j.fsi.2018.12.041.

Li, Y., et al. 2015. Histamine levels in embryonic chicken livers infected with very virulent infectious bursal disease virus. *Vet Immunol Immunopathol*. 168,91-96.https://doi.org/10.1016/j.vetimm.2015.08.012.

Lin, J., et al. 2016. Genome-wide profiling of chicken dendritic cell response to infectious bursal disease. *BMC Genomics*. 17,878.https://doi.org/10.1186/s12864-016-3157-5.

Lin, J., et al. 2019. Medium optimization based on comparative metabolomic analysis of chicken embryo fibroblast DF-1 cells. *RSC Advances*. 9,27369-27377.https://doi.org/10.1039/c9ra05128g.

Liste-Calleja, L., et al. 2014. HEK293 cell culture media study towards bioprocess optimization: Animal derived component free and animal derived component containing platforms. *Journal of Bioscience and Bioengineering*. 117,471-477.https://doi.org/10.1016/j.jbiosc.2013.09.014.

Liu, Y., et al. 2005. Preparation of ChIL-2 and IBDV VP2 fusion protein by baculovirus expression system. *Cellular & molecular immunology*. 2,231-235.

Luo, C., et al. 2018. Dynamic analysis of expression of chemokine and cytokine gene responses to H5N1 and H9N2 avian influenza viruses in DF-1 cells. *Microbiology and Immunology*. 62,327-340.https://doi.org/10.1111/1348-0421.12588.

Moresco, K.A., et al. 2010. Evaluation and Attempted Optimization of Avian Embryos and Cell

Culture Methods for Efficient Isolation and Propagation of Low Pathogenicity Avian Influenza Viruses. *Avian Diseases*. 54,622-626.https://doi.org/10.1637/8837-040309-Reg.1.

Muller, H., et al. 2003. Research on infectious bursal disease - the past, the present and the future. *Veterinary Microbiology*. 97,153-165.https://doi.org/10.1016/j.vetmic.2003.08.005.

Muller, H., et al. 2012. Current status of vaccines against infectious bursal disease. *Avian Pathol*. 41,133-139.https://doi.org/10.1080/03079457.2012.661403.

Munger, J., et al. 2006. Dynamics of the cellular metabolome during human cytomegalovirus infection. *PLoS Pathog*. 2,e132.https://doi.org/10.1371/journal.ppat.0020132.

Niu, X., et al. 2017. Transcriptome analysis of avian reovirus-mediated changes in gene expression of normal chicken fibroblast DF-1 cells. *BMC Genomics*. 18,911.https://doi.org/10.1186/s12864-017-4310-5.

Noor, M. 2009. Development of infectious bursal disease virus vaccine candidates by reverse genetics. *PhD Thesis, Bangladesh Agricultural University*.

Noor, M., et al. 2014. Further evidence for the association of distinct amino acid residues with in vitro and in vivo growth of infectious bursal disease virus. *Arch Virol*. 159,701-709.https://doi.org/10.1007/s00705-013-1885-2.

Quan, R., et al. 2017. Transcriptional profiles in bursal B-lymphoid DT40 cells infected with very virulent infectious bursal disease virus. *Virol J*. 14,7.https://doi.org/10.1186/s12985-016-0668-2.

Reed, L.J., and H. Muench. 1938. A Simple Method of Estimating Fifty Per Cent Endpoints12.

American Journal of Epidemiology. 27,493-497.https://doi.org/10.1093/oxfordjournals.aje.a118408.

Rekha, K., et al. 2014. Growth and replication of infectious bursal disease virus in the DF-1 cell line and chicken embryo fibroblasts. *Biomed Res Int*. 2014,494835.https://doi.org/10.1155/2014/494835.

Sakamoto, H., et al. 2005. Host sphingolipid biosynthesis as a target for hepatitis C virus therapy. *Nat Chem Biol*. 1,333-337.https://doi.org/10.1038/nchembio742.

Sanchez, E.L., and M. Lagunoff. 2015. Viral activation of cellular metabolism. *Virology*. 479-480,609-618.https://doi.org/10.1016/j.virol.2015.02.038.

Schaefer-Klein, J., et al. 1998. The EV-O-derived cell line DF-1 supports the efficient replication of avian leukosis-sarcoma viruses and vectors. *Virology*. 248,305-311.https://doi.org/10.1006/viro.1998.9291.

Schaefer, E.A., and R.T. Chung. 2013. HCV and host lipids: an intimate connection. *Seminars in liver disease*. 33,358-368.https://doi.org/10.1055/s-0033-1358524.

Schoeman, J.C., et al. 2016. Metabolic characterization of the natural progression of chronic hepatitis B. *Genome Med.* 8,13.https://doi.org/10.1186/s13073-016-0318-8.

Shen, C.F., et al. 2012. Process optimization and scale-up for production of rabies vaccine live adenovirus vector (AdRG1.3). *Vaccine*. 30,300-306.https://doi.org/10.1016/j.vaccine.2011.10.095.

Silva, A.C., et al. 2016. Impact of Adenovirus infection in host cell metabolism evaluated by (1)H-NMR spectroscopy. *J Biotechnol*. 231,16-23.https://doi.org/10.1016/j.jbiotec.2016.05.025.

Vastag, L., et al. 2011. Divergent effects of human cytomegalovirus and herpes simplex virus-1 on cellular metabolism. *PLoS Pathog*. 7,e1002124.https://doi.org/10.1371/journal.ppat.1002124.

Wang, B., et al. 2015. Comparative metabolic profiling reveals the key role of amino acids metabolism in the rapamycin overproduction by Streptomyces hygroscopicus. *J Ind Microbiol Biotechnol*. 42,949-963.https://doi.org/10.1007/s10295-015-1611-z.

Xia, J., and D.S. Wishart. 2016. Using MetaboAnalyst 3.0 for Comprehensive Metabolomics Data Analysis. *Curr Protoc Bioinformatics*. 55,14 10 11-14 10 91.https://doi.org/10.1002/cpbi.11.

Xiong, W., et al. 2017. Phosphorylation of Icariin Can Alleviate the Oxidative Stress Caused by the Duck Hepatitis Virus A through Mitogen-Activated Protein Kinases Signaling Pathways. *Front Microbiol*. 8,1850.https://doi.org/10.3389/fmicb.2017.01850.

Yip, C.W., et al. 2012. Cell culture-adapted IBDV uses endocytosis for entry in DF-1 chicken embryonic fibroblasts. *Virus Res*. 165,9-16.https://doi.org/10.1016/j.virusres.2011.12.016.

ŽIvkov BaloŠ, M., et al. 2019. The role, importance and toxicity of arsenic in poultry nutrition. *World's Poultry Science Journal*. 75,375-386.https://doi.org/10.1017/s0043933919000394.

Data

Figure 1

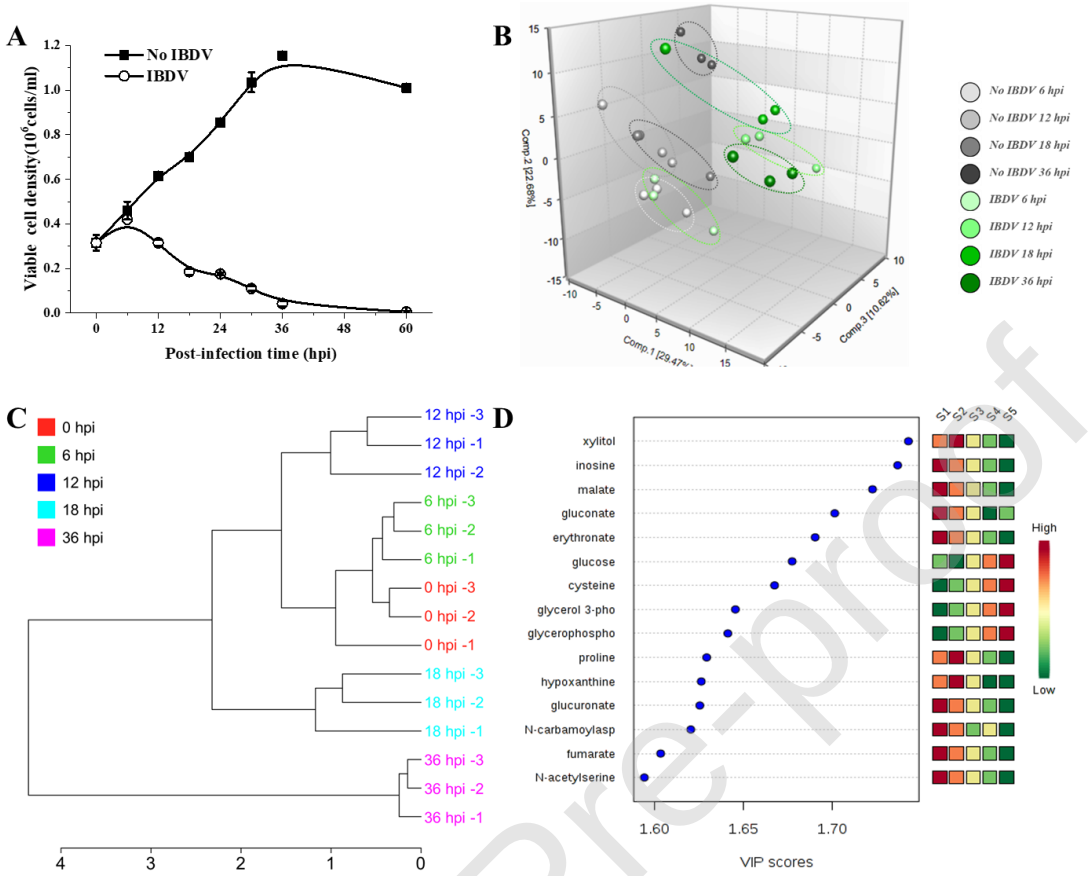

Differential and time series analysis of the metabolic profiles of the cultures. (A) Viable cell density of DF-1 cells infected with IBDV (IBDV) and without infection (no IBDV). (B) Three-dimensional principal component analysis (PCA) plot of 193 metabolite features. Comp.1 accounted for 29.47% of the variation among the eight groups, and Comp.2 accounted for 22.68%. DF-1 cells were mock infected (no IBDV, gray circle) or were virally infected (IBDV, green circle) for 6, 12, 18, and 36 hpi. The cells were then harvested for metabolomic profiling, and three biological replicates of each group were provided. Application of PCA provided by Metabolon to determine the separation of individual samples as a function of cellular metabolites revealed fairly distinct separation between mock-infected cells and IBDV-infected cells at different time points, predicting a strong shift in the metabolic profiles among the two groups. (C) and (D) DF-1 cells were IBDV infected for 0, 6, 12, 18, and 36 hours, and then were harvested for statistical analysis by MetaboAnalyst. Three biological replicates of each group were provided. (C) Hierarchical clustering displaying the feature expression pattern shown as a dendrogram (distance measure using Pearson's correlation, and clustering algorithm using Ward.D clustering to minimize the sum of squares of any two clusters). DF-1 cells were IBDV-infected for 0, 6, 12, 18, and 36 hours. (D), Important features identified by PLS-DA. The colored boxes on the right indicate the relative concentrations of the corresponding metabolite in each group, and S1-S5 indicate the 5 sample groups from 0-36 hpi, respectively.

Figure 2

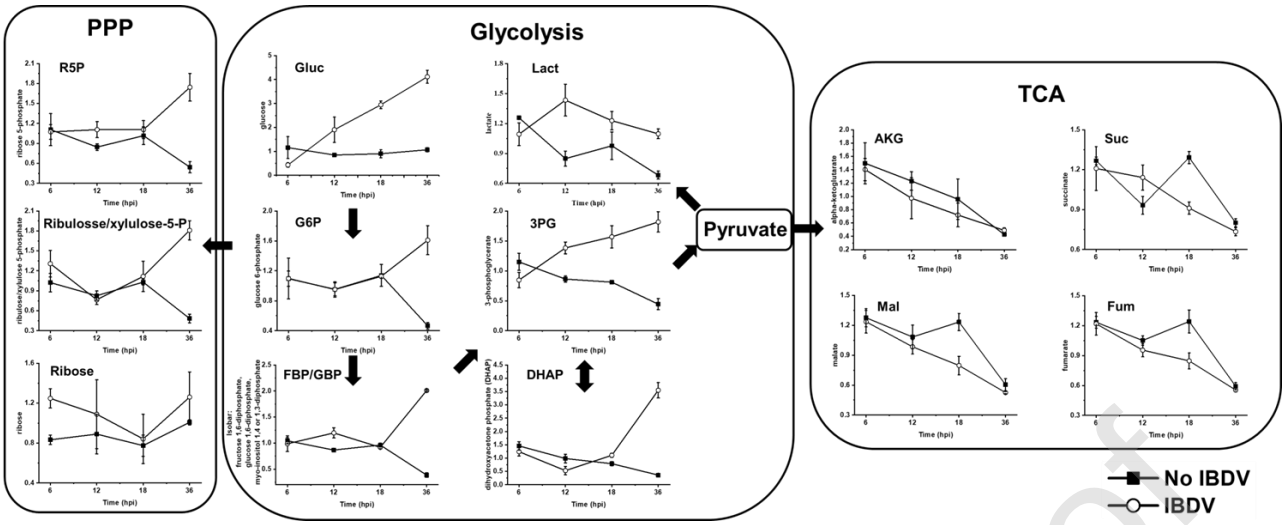

IBDV-induced changes in central carbon metabolites. The line graph represents the metabolites that have undergone significant changes detected in glycolysis, TCA, and PPP. Replicate cultures of DF-1 cells were mock-infected (no IBDV, solid square) or virally infected with IBDV (IBDV, open circle). Cells were harvested at 6, 12, 18, 36 hpi and were processed for GC-MS and UPLC-MS/MS. Raw area counts from three independent experiments performed in triplicate (n = 3) were normalized to protein levels. Error bars show ±1 s.d. of the mean.

Figure 3

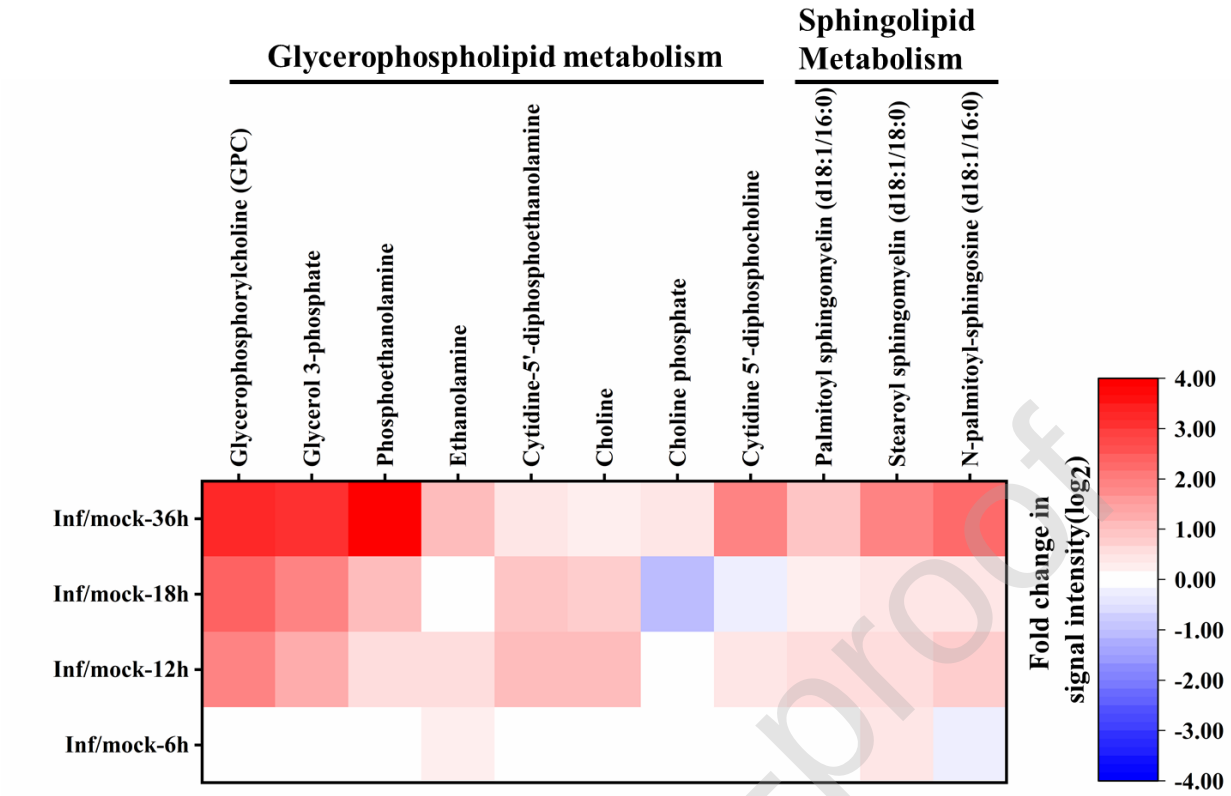

IBDV-induced changes in glycerophospholipid and sphingolipid metabolites. Glycerophospholipid and sphingolipid metabolite profiles of DF-1 cells mock infected or virally infected with IBDV at 6, 12, 18, and 36 hpi were shown as a heatmap. Increased metabolite concentrations are shown in red, whereas decreased metabolite concentrations are shown in blue.

Figure 4

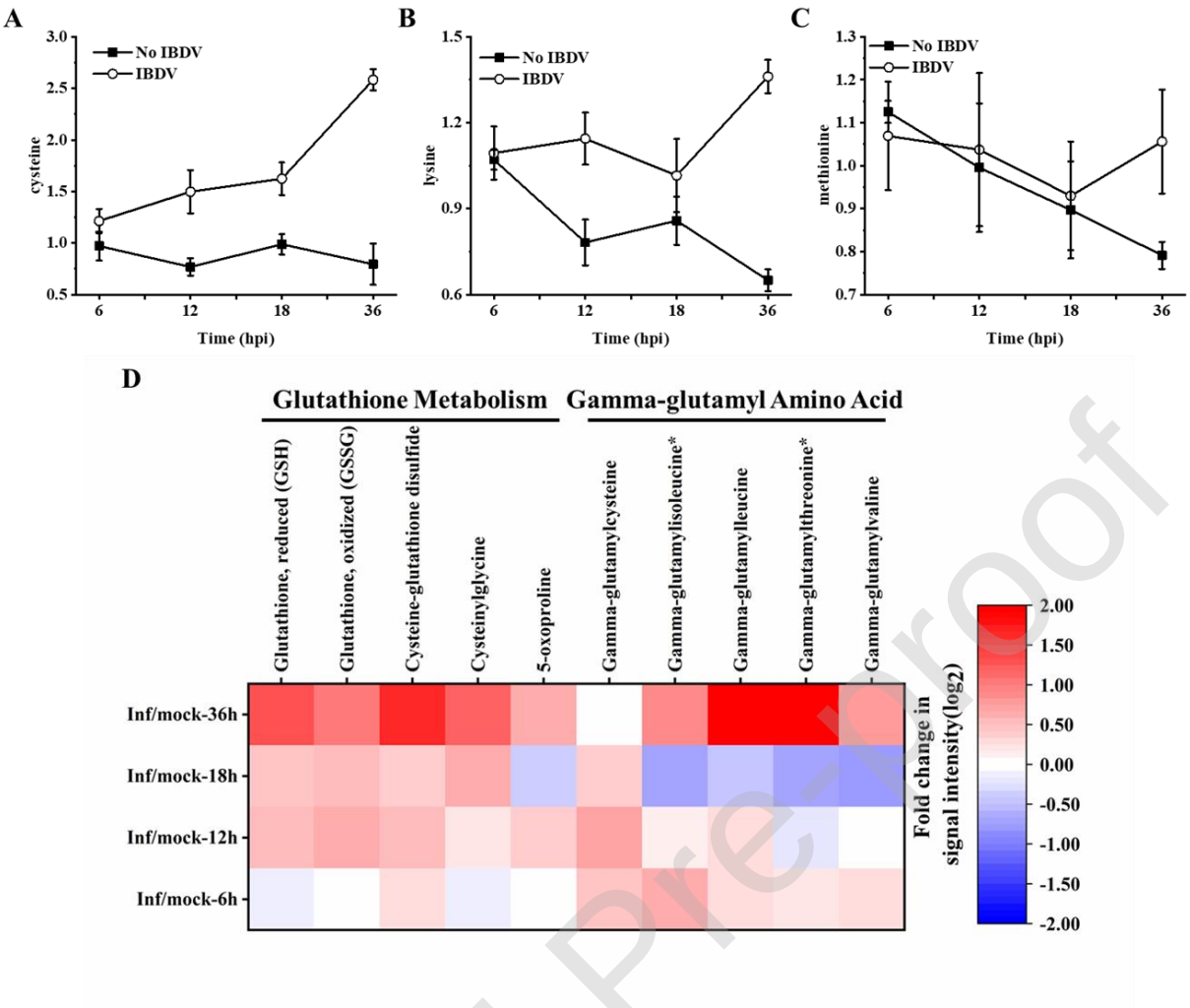

IBDV-induced changes in amino acid metabolites. (A), (B), and (C) show a significant increase in cysteine, lysine, and methionine levels in cells infected with IBDV (IBDV, open circle) for 12, 18 and 36 hours compared with uninfected controls (no IBDV, solid square). Raw area counts from three independent experiments performed in triplicate (n = 3) were normalized to protein levels. Error bars show ±1 s.d. of the mean. D shows the glutathione pathway metabolite profiles of DF-1 cells mock-infected or virally infected with IBDV at 6, 12, 18, and 36 hpi were shown as a heatmap. Increased metabolite concentrations are shown in red, whereas decreased metabolite concentrations are shown in blue.

Figure 5

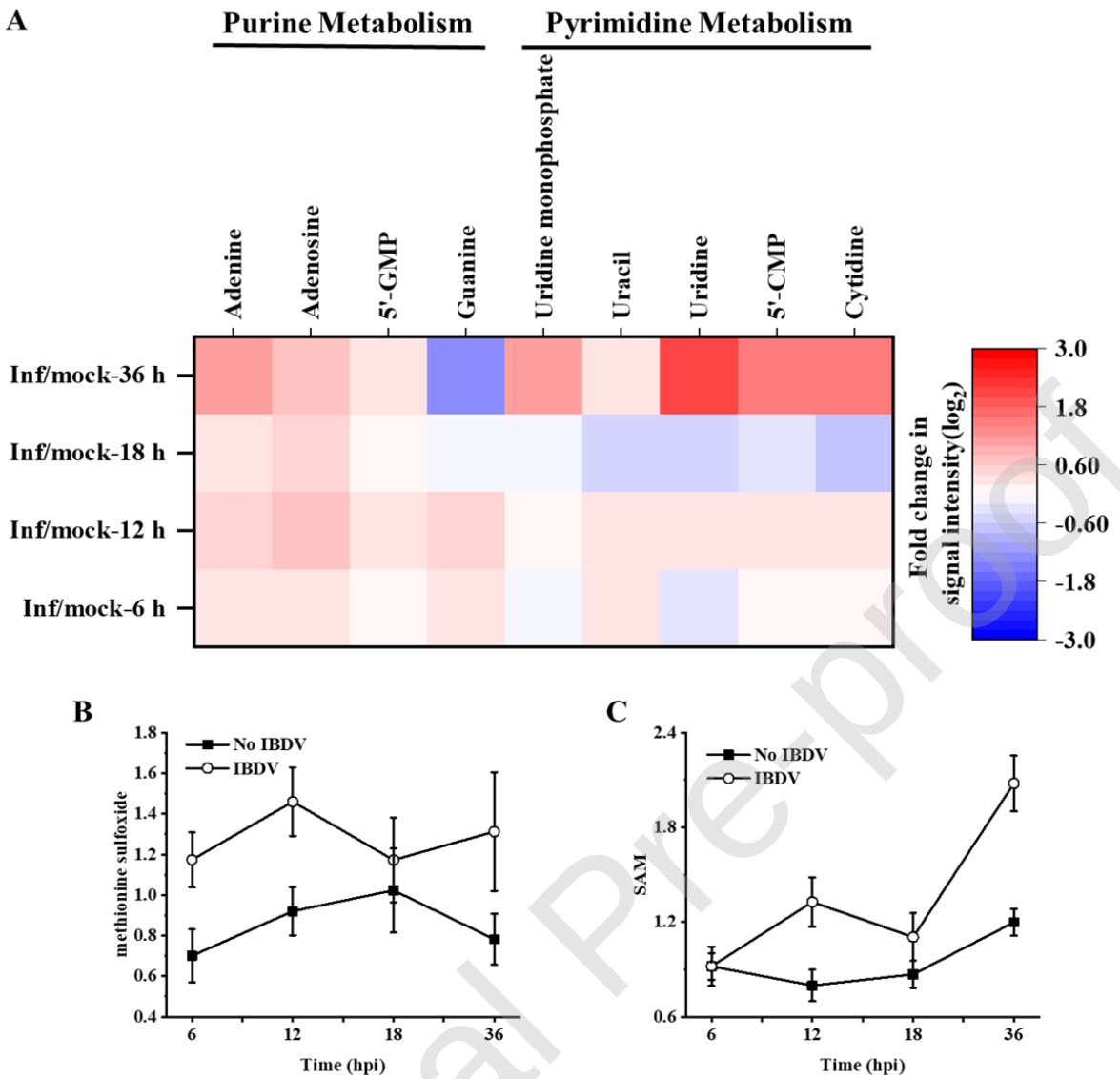

IBDV-induced changes in nucleoside metabolites. (A) show purine and pyrimidine metabolite profiles of DF-1 cells mock-infected or virally infected with IBDV at 6, 12, 18, and 36 hpi and shown as a heatmap. Increased metabolite concentrations are shown in red, whereas decreased metabolite concentrations are shown in blue. (B) and (C) show a significant increase in the methionine sulfoxide and SAM levels in cells infected with IBDV (IBDV, open circle) for 12, 18 and 36 hours compared with uninfected controls (no IBDV, solid square). Raw area counts from three independent experiments performed in triplicate (n = 3) were normalized to the protein levels. Error bars show ±1 s.d. of the mean.

Figure 6

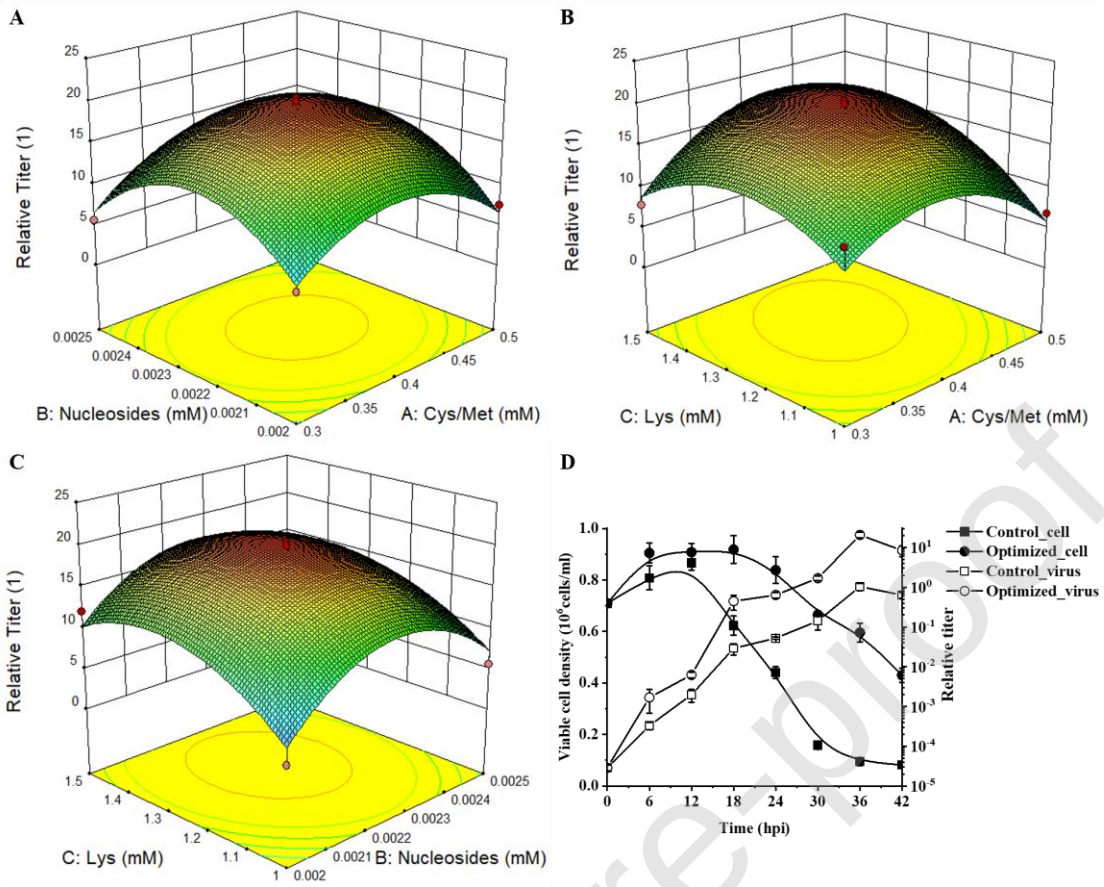

Three-dimensional curved surfaces of the mutual influence on IBDV propagation for three factors in BBD experiments and comparison of the production between optimized and control media. (A) Effects of nucleoside and Cys/Met groups; (B) effects of Lys and Cys/Met groups; (C) effects of Lys and nucleoside groups; (D) comparison of the IBDV propagation and the DF-1 cell growth between optimized and control media. N = 3 biological replicates, and error bars represent s.d.

Table 1 Intracellular differential metabolites and metabolic pathways involved in mock- or IBDV-infected DF-1 cell

Component	Style	Sub Pathway	12 hpi		18 hpi		36 hpi	
			FC	p.value	FC	p.value	FC	p.value
glycerol 3-phosphate	Lipid	Glycerolipid Metabolism	0.43	0.0001	0.25	0.0003	0.11	0.0001
glycerophosphorylcholine GPC	Lipid	Phospholipid Metabolism	0.27	0.0002	0.19	0.0001	0.1	0.0001
glycine	Amino Acid	Glycine, Serine and Threonine Metabolism	2.58	0.0003	2.84	0.0009	2.66	0.0002
xylitol	Carbohydrate	Pentose Metabolism	2.72	0.0009	11.26	0	14.96	0.0002
gluconate	Xenobiotics	Food Component/Plant	2.31	0.0023	4.93	0.0024	4.25	0.0001
pantothenate	Cofactors and Vitamins	Pantothenate and CoA Metabolism	2.29	0.0024	4.48	0.0001	2.36	0
sorbitol	Carbohydrate	Fructose, Mannose and Galactose Metabolism	2.04	0.0038	4.89	0.0016	2.55	0.0008
sarcosine	Amino Acid	Glycine, Serine and Threonine Metabolism	3.58	0.0072	4.1	0.0026	12.45	0.0008
glucuronate	Carbohydrate	Aminosugar Metabolism	2.5	0.0111	4.46	0.0014	6.54	0
citrulline	Amino Acid	Urea cycle; Arginine and Proline Metabolism	0.4	0.0132	0.36	0.0026	0.17	0.0002
cadaverine	Amino Acid	Lysine Metabolism	2.68	0.0219	11.93	0.0006	7.59	0
fructose	Carbohydrate	Fructose, Mannose and Galactose Metabolism	0.38	0.0348	0.27	0.0086	0.09	0
arabitol	Carbohydrate	Pentose Metabolism	2.54	0.0439	3.18	0.0919	2.92	0.0019
glucose	Carbohydrate	Glycolysis, Gluconeogenesis, and Pyruvate Metabolism	0.45	0.0784	0.31	0.0041	0.26	0.0002

Table 2 Metabolic pathway analysis of DF-1 cells infected with IBDV

Style	Pathway [a]	Raw p [b]	Impact [c]
Lipid	Glycerophospholipid metabolism	1.89E-09	0.24
Amino Acid	Glutathione metabolism	4.91E-09	0.59
Lipid	Sphingolipid metabolism	6.80E-07	0.30
Energy	Citrate cycle (TCA cycle)	8.16E-07	0.26
Amino Acid	Arginine and proline metabolism	1.02E-06	0.52
Carbohydrate	Fructose and mannose metabolism	1.11E-05	0.24
Cofactors and Vitamins	Pentose phosphate pathway	1.54E-05	0.32
Nucleotide	Purine metabolism	2.06E-05	0.42
Amino Acid	Cysteine and methionine metabolism	4.40E-05	0.54
Carbohydrate	Starch and sucrose metabolism	5.32E-05	0.31
Nucleotide	Nicotinate and nicotinamide metabolism	2.80E-04	0.49
Lipid	Steroid biosynthesis	6.88E-04	0.35
Amino Acid	beta-Alanine metabolism	7.10E-04	0.45
Amino Acid	Alanine, aspartate and glutamate metabolism	7.87E-04	0.78
Amino Acid	Glycine, serine and threonine metabolism	1.28E-03	0.59
Carbohydrate	Pentose and glucuronate interconversions	1.29E-03	0.67
Other	Aminoacyl-tRNA biosynthesis	1.72E-03	0.19
Carbohydrate	Galactose metabolism	5.94E-03	0.48
Nucleotide	Pyrimidine metabolism	8.19E-03	0.30
Amino Acid	Histidine metabolism	9.06E-03	0.27
Cofactors and Vitamins	Pantothenate and CoA biosynthesis	1.31E-02	0.47
Cofactors and Vitamins	Ascorbate and aldarate metabolism	2.39E-02	0.20
Amino Acid	Lysine biosynthesis	2.65E-02	0.30
Carbohydrate	Amino sugar and nucleotide sugar metabolism	3.40E-02	0.20

[a] The pathway analysis module uses KEGG metabolic pathways as the backend knowledgebase.

[b] Raw p is the original p value calculated from the enrichment analysis based on GlobalTest.

[c] Impact is the pathway impact value calculated from pathway topology analysis.

Table 3 Two coded levels of variables investigated using PBD and the contribution of components

Term	Group	Components	Concentration (mM)		Effect	% Contribution
			-1	1		
A	amino acid 1	arginine	0.6991	1.3981	-0.92	4.49
		proline	0.1500	0.3000		
		glycine	0.2500	0.5000		
B	amino acid 2	serine	0.2500	0.5000	-0.51	1.37
		threonine	0.4492	0.8983		
C	amino acid 3	aspartate	0.0500	0.1000	0.17	0.15
D	amino acid 4	alanine	0.2500	0.5000	0.17	0.15
E	amino acid 5	glutamine	2.5000	5.0000	0.68	2.41
F	amino acid 6	cysteine	0.0998	0.1995	2.52	33.51
		methionine	0.1157	0.2314		
G	amino acid 7	lysine	0.4986	0.9973	1.60	13.47
H	nucleotides	nucleotides	0.0015	0.0030	1.77	16.43

Table 4 Matrix and experimental responses of PBD with N = 11

Run [a]	amino acid 1	amino acid 2	amino acid 3	amino acid 4	amino acid 5	amino acid 6	amino acid 7	nucleotides	dummy 1	dummy2	dummy3	Response
	A	B	C	D	E	F	G	H	J	K	L	Relative titer
1	1	1	-1	1	1	1	-1	-1	-1	1	-1	1.5
2	-1	1	-1	1	1	-1	1	1	1	-1	-1	6.3
3	1	-1	1	1	-1	1	1	1	-1	-1	-1	6.3
4	1	-1	1	1	1	-1	-1	-1	1	-1	1	3.53
5	1	1	-1	-1	-1	1	-1	1	1	-1	1	6.3
6	-1	-1	-1	1	-1	1	1	-1	1	1	1	6.3
7	-1	1	1	1	-1	-1	-1	1	-1	1	1	2
8	1	1	1	-1	-1	-1	1	-1	1	1	-1	1.5
9	1	-1	-1	-1	1	-1	1	1	-1	1	1	3.53
10	-1	-1	-1	-1	-1	-1	-1	-1	-1	-1	-1	1
11	-1	1	1	-1	1	1	1	-1	-1	-1	1	6.3
12	-1	-1	1	-1	1	1	-1	1	1	1	-1	6.3

[a] The levels in Table 4 are the same as those described in Table 3.

Table 5 Runs and responses of the path of the steepest ascent design

Run	Cys/Met	Nucleosides	Lys	Relative Titer
	mM	mM	mM	
1	0.2	0.00175	0.75	2.00 ±0.23
2	0.3	0.002	1	15.40 ±2.86
3	0.4	0.00225	1.25	19.95 ±2.30
4	0.5	0.0025	1.5	14.62 ±2.88
5	0.6	0.00275	1.75	2.66 ±0.46

Table 6 Matrix and experimental and predicted responses of BBD

Run	Level	A: Cys/Met	B: Nucleosides	C: Lys	Relative Titer	
		mM	mM	mM	Predicted	Experimental
	-1	0.3	0.002	1		
	0	0.4	0.00225	1.25		
	1	0.5	0.0025	1.5		
1		0	0	0	19.7	20.45 ±3.67
2		0	0	0	19.7	19.95 ±1.83
3		0	0	0	19.7	18.70 ±1.74
4		-1	0	-1	9.37	11.97 ±5.88
5		-1	1	0	6.58	5.66 ±0.03
6		-1	0	1	8.84	7.81 ±2.19
7		0	-1	1	10.39	12.06 ±2.06
8		1	0	1	14.41	11.82 ±3.52
9		-1	-1	0	7.42	6.78 ±1.16
10		0	1	-1	7.29	5.62 ±1.40
11		1	-1	0	6.59	7.51 ±0.43

12	0	1	1	10.49	12.44	±2.93
13	1	1	0	9.36	10.00	±1.25
14	1	0	-1	5.75	6.78	±1.16
15	0	-1	-1	5.46	3.50	±0.96